

PCCP

Accepted Manuscript



This is an *Accepted Manuscript*, which has been through the Royal Society of Chemistry peer review process and has been accepted for publication.

Accepted Manuscripts are published online shortly after acceptance, before technical editing, formatting and proof reading. Using this free service, authors can make their results available to the community, in citable form, before we publish the edited article. We will replace this *Accepted Manuscript* with the edited and formatted *Advance Article* as soon as it is available.

You can find more information about *Accepted Manuscripts* in the [Information for Authors](#).

Please note that technical editing may introduce minor changes to the text and/or graphics, which may alter content. The journal's standard [Terms & Conditions](#) and the [Ethical guidelines](#) still apply. In no event shall the Royal Society of Chemistry be held responsible for any errors or omissions in this *Accepted Manuscript* or any consequences arising from the use of any information it contains.

Large-scale Superhydrophobic Surface-enhanced Raman Scattering (SERS) Platform Fabricated via Capillary Force Lithography and Assembly of Ag Nanocubes for Ultratrace Molecular Sensing

Joel Ming Rui Tan,^{^,†,#} Justina Jiexin Ruan,^{†,#} Hiang Kwee Lee,^{†,≠} In Yee Phang,[≠] Xing Yi Ling^{†*}

[†] *Division of Chemistry and Biological Chemistry, School of Physical and Mathematical Sciences, Nanyang Technological University, 21 Nanyang Link, Singapore 637371.*

[≠] *Institute of Materials Research and Engineering, A*STAR (Agency for Science, Technology and Research), 3 Research Link, Singapore 117602.*

[^] *Interdisciplinary Graduate School, Nanyang Technological University, Singapore.*

[#] *These authors contributed equally.*

^{*} *To whom correspondence should be addressed. Email: xyling@ntu.edu.sg.*

KEYWORDS: superhydrophobic, surface enhanced Raman scattering, plasmonic, silver nanocube, ultratrace molecular detection, capillary force lithography.

Abstract

An analytical platform with ultratrace detection limit in atto-molar (aM) concentration range is vital for forensic, industrial and environment sectors that handle scarce/ highly toxic samples. Superhydrophobic surface-enhanced Raman scattering (SERS) platforms serve as an ideal platform to enhance detection sensitivity by reducing the random spreading of aqueous solution. However, the fabrication of superhydrophobic SERS platforms is generally limited due to the use of sophisticated and expensive protocols and/or suffers structural/signal inconsistency. Herein, we demonstrate a high-throughput fabrication of stable and uniform superhydrophobic SERS platform for ultratrace molecular sensing. Large-area box-like micropatterns of polymeric surface are first fabricated using capillary force lithography (CFL). Subsequently, plasmonic properties are incorporated onto the patterned surfaces by decorating with Ag nanocubes using Langmuir-Schaefer technique. To create a stable superhydrophobic SERS platform, an additional 25-nm Ag film is coated over the Ag nanocube-decorated patterned template followed by chemical functionalization with perfluorodecanethiol. Our resulting superhydrophobic SERS platform demonstrates excellent water-repellency with a water contact angle of $165^\circ \pm 9^\circ$ and a consequent analyte concentrating factor of 57-folds, as compared to its hydrophilic counterpart. By combining the analyte concentrating effect of superhydrophobic surfaces with intense the intense electromagnetic “hot spots” of Ag nanocubes, our superhydrophobic SERS platform achieves an ultra-low detection limit of 10^{-17} M (10 aM) for rhodamine 6G using just 4 μ L of analyte solutions, corresponding to an analytical SERS enhancement factor of 10^{13} . Our fabrication protocol demonstrates a simple, cost- and time-effective approach in the large-scale fabrication of superhydrophobic SERS platform for ultratrace molecular detection.

Introduction

Surface-enhanced Raman scattering (SERS) is an ultrasensitive spectroscopic technique capable of providing characteristic molecular vibrational fingerprint even at trace concentration.¹ This unique property renders SERS an extremely useful sensing tool extensively applied in industrial and environmental safety and also bio-imaging.²⁻⁵ The ultra-sensitivity of SERS is attributed to the intense electromagnetic field that is confined near the metal nanoparticles, as a result of coherent oscillation of electrons in the metal nanoparticles with the incident light.^{6, 7} Studies showed that regions with most intense localized electromagnetic fields, commonly termed as “hot-spots”, are located at the tips/vertices of plasmonic nanostructures and also in the gaps between adjacent plasmonic nanostructures. Hence, close-packed assembly of anisotropic noble metal nanoparticles (Ag or Au) poses an ideal candidate for highly sensitive SERS analytical platform.⁸ Despite the ultra-sensitivity of SERS,⁸⁻¹⁰ the random spreading of aqueous analyte on conventional hydrophilic SERS platform dilutes analyte molecules.^{11, 12} The process of dilution lowers the SERS detection sensitivity and hence is a challenge for the detection of minute amounts of analyte.

Superhydrophobicity overcomes the random spreading issue by confining substrate-water interface into a much smaller area compared to a hydrophilic platform.^{13, 14} Hence, higher analyte-to-area ratios, ranging from 4-folds to 9-folds increment, have been reported to enhance SERS detection sensitivity for ultratrace molecular sensing.¹³⁻¹⁷ Superhydrophobic surface typically possesses hierarchical micro- and/or nano-scale surface roughness and hydrophobic surface functionality, which exhibits a static water contact angle of more than 150°.^{16, 18, 19} Commonly, superhydrophobic SERS platforms are fabricated by incorporating plasmonic properties onto as-prepared superhydrophobic platform via decoration with Ag or Au nanoparticles.^{14, 20} For instance, the electrode-less deposition of polycrystalline Ag film on surfaces patterned by electron beam and/or photo-lithography has achieved a detection limit of attomolar (10^{-18} M) detection of rhodamine 6G.²¹ However, the need of expensive and sophisticated equipment limits its practicality for routine usage. Alternatively, superhydrophobic SERS platform fabricated via thermal evaporation of Ag film on dried rose petal has also been exploited, with detection of rhodamine 6G

down to nanomolar (10^{-9} M) level.¹³ Although the use of widely abundant rose petal is cost-effective and present a large-scale fabrication of superhydrophobic SERS platform, this method may suffer from weak Raman signal enhancement due to the use of polycrystalline Ag film. Hence, the development of a cost- and time-effective fabrication of large-scale, homogenous and sensitive SERS platform is essential, especially for routine ultratrace sensing application in the field of forensics, industrial and environmental safety.

Herein, we demonstrate the fabrication of a large-scale superhydrophobic SERS platform and its application for ultratrace molecular sensing. Our strategy combines the analyte concentrating effect imparted by superhydrophobicity, and high density of electromagnetic “hot-spots” provided by a compact assembly of Ag nanocubes. Capillary force lithography (CFL) is first employed to create large-scale and homogeneous periodic micro-scale roughness essential for superhydrophobicity. Subsequent assembly of Ag nanoparticles on the patterns using Langmuir-Schaefer technique provides both plasmonic properties and nano-scale roughness. A layer of Ag film is evaporated over the assembled Ag nanocube to improve stability of the Ag nanocubes and subsequently grafted with perfluorodecanethiol to achieve superhydrophobicity. The hydrophobicity of our patterned platform at various fabrication stages will be systematically examined. We then quantitatively determine the analyte concentrating effect, the detection limit of the analyte, the analytical enhancement factor of our superhydrophobic SERS platform as well as demonstrating its superiority over hydrophilic platform.

Results and discussion

Large-scale ($1\text{ cm} \times 1\text{ cm}$) and homogeneous periodic box-like micropatterns are fabricated via capillary force lithography at elevated temperature to generate micro-scale roughness essential for superhydrophobicity (Figure 1a). Linearly-patterned Si master ($1 \times 1\text{ cm}$ patterned area containing $5\text{ }\mu\text{m}$ wide, $1\text{ }\mu\text{m}$ tall horizontal pillars and $3\text{ }\mu\text{m}$ periodicity linear pillars) are first imprinted onto a 200 nm poly(methylmethacrylate) (PMMA) film at $200\text{ }^\circ\text{C}$, and subsequently rotated 90° and imprinted again to form the periodic box-like patterns. The first imprinting yields distinct linear micropatterns of $5\text{ }\mu\text{m}$ in width, 200 nm in thickness and 650 nm tall protrusions wall (Figure S1) at both edges owing to PMMA conforming to the wall of the mask during the compression process (Figure 1b). Subsequent imprinting generates periodic box-like micropatterns (termed “patterned template”) of $5 \times 5\text{ }\mu\text{m}$ in size with $3\text{ }\mu\text{m}$ periodicity, 200 nm in thickness, 650 nm tall protrusions walls on all four sides of the box (Figure 1c and d). The formation of such box-like morphology is due to the capillary force driving PMMA to conform to the master mold pattern.²² The as-prepared patterned template are then coated with a 2-nm alumina (Al_2O_3) layer to enhance both stability against organic solvents and also wettability for subsequent fabrication of large-scale homogeneous superhydrophobic SERS platform.

Ag nanocubes are then assembled onto the patterned template to install both nano-scale roughness and also plasmonic properties essential for latter SERS application. Ag nanocubes are first synthesized using the polyol method²³ in high yield with monodisperse edge lengths of $127 \pm 11\text{ nm}$ and characteristic localized surface plasmon resonances²⁴ (LSPRs) are observed in the visible spectrum (Figure S2). For the assembly, Ag nanocubes are first suspended at the water/air interface and then transferred onto the patterned template via Langmuir-Schaefer technique (Figure 2).^{25, 26} Generally, we observe a dense monolayer of Ag nanocubes deposited on the exterior and walls of the box-like structures while multilayer aggregations of Ag nanocubes are formed within the boxes. Such selective aggregation of Ag nanocubes within the boxes is mainly due to the strong capillary interaction between water,²⁷ on which Ag nanocubes are suspended, with the alumina-coated patterned template (refer to Supporting Information for detailed discussion). Hence, high density of

electromagnetic “hot-spots” can be created, which is essential for latter ultratrace SERS sensing application. The assembled Ag nanocubes on the patterned template are then stabilized against re-dispersal by coating an additional 25-nm Ag film via thermal evaporation.¹⁵

To highlight the importance of hierarchical structures on superhydrophobicity, we quantitatively compare the root-mean-square (rms) surface roughness of flat, linear, patterned template and Ag nanocube-decorated patterned template using atomic force microscopy (AFM). A flat 200-nm PMMA layer is observed to have negligible surface roughness of ~ 0.3 nm. After imprinting, the rms roughness increases at least 550-folds, to 167 nm and 247 nm after the first (linear arrays) and second imprinting (box-like patterned template), respectively (Figure 3a, Table 1). Subsequent decoration of patterned template with Ag nanocubes further enhances surface roughness to 341 nm (Figure 3a). Hence, the need of hierarchical structures, comprising of micro-scale patterned template and nano-scale Ag nanocubes, is clearly evident in achieving highly rough asperities essential for superhydrophobicity.

Superhydrophobicity is conferred to the Ag nanocube-decorated patterned template via the grafting of hydrophobic perfluorodecanethiol molecules onto the Ag surfaces. The Ag nanocube-decorated patterned templates are observed to demonstrate excellent water-repelling properties with static water contact angle of $\geq 165^\circ$ (Figure 3, Table 1), which indicates that superhydrophobicity has been achieved. In contrary, Ag nanocube-decorated patterned templates without hydrophobic perfluorodecanethiol moiety only exhibit a static contact angle of $143^\circ \pm 2^\circ$, which is still 7° short from superhydrophobicity and 21° lower compared to the perfluorodecanethiol-grafted counterpart. The results therefore clearly emphasize the importance of hydrophobic chemical functionality to achieve superhydrophobicity.

Similarly, surface roughness is also observed to be a major factor in the fabrication of superhydrophobic surface where a flat, linearly-patterned and box-like patterned template of bare PMMA, previously demonstrated to have lower surface roughness, exhibits a much lower static contact angles of $111^\circ \pm 4^\circ$, $124^\circ \pm 5^\circ$ and $106^\circ \pm 5^\circ$, respectively (Table 1, refer to Supporting Information for detailed discussion). Hence, both findings agree well with the fundamental, which

indicate that both surface chemical functionality and hierarchical micro-/nano-scale roughness are essential for superhydrophobicity.²⁸⁻³⁰ The necessity of hierarchical Ag nanocube-decorated patterned template for the fabrication of superhydrophobic platform is re-emphasized by the homogeneity of hydrophobicity along both x- and y-axis, as compared to bare PMMA patterns which demonstrate asymmetric contact angles along the two axes instead (Figure S3). Hence, from here onwards, perfluorodecanethiol-functionalized Ag nanocube-decorated patterned templates are used as the superhydrophobic SERS platform due to its superior surface roughness and superhydrophobicity.

Contact angle hysteresis is quantified to examine the water adhesion property of the superhydrophobic SERS platform. By taking the difference between advancing and receding contact angles, the value of the contact angle hysteresis can further enhance the analyte concentration effect on the surface. Typically, a surface with higher contact angle hysteresis exhibits greater adhesion/pinning of water droplet to the surface, whereas a surface with lower contact angle hysteresis exhibits greater tendency of rolling off water droplets. Our Ag nanocube-decorated patterned templates exhibit moderate contact angle hysteresis of $35^\circ \pm 9^\circ$ (Table 1), indicating a surface adhesion characteristic between that of lotus-like surface ($< 10^\circ$, low adhesion) and rose-petal-like surface ($> 90^\circ$, high adhesion). This intermediate adhesion property allows moderate pinning of aqueous analyte droplets onto the superhydrophobic SERS platform for high throughput analysis and also a greater analyte concentrating effect as the three-phase contact line recedes upon drying.

To demonstrate the aqueous analyte concentrating effect essential for enhancing SERS detection sensitivity, we analyze the contact areas of 4- μ L water droplets on both the superhydrophobic SERS platform and a hydrophilic O₂-plasma-treated Si substrate. The 4- μ L water droplet readily spreads across a hydrophilic surface, giving rise to a thin water film with static contact angle of $< 20^\circ$ and contact diameter of 5.37 mm (Figure 4a, 4d). On the other hand, the 4- μ L water droplet is strongly repelled by the superhydrophobic surface, giving rise to a spherical water droplet with high static contact angle of $164^\circ \pm 5^\circ$ and a contact diameter of 0.70 mm (Figure 4b, 4e) achieving a $7.7 \times$

decrease in contact diameter. Hence, the corresponding maximum water-surface contact area on superhydrophobic surface is approximately 58.9-fold lesser than its hydrophilic counterpart. This indicates that our superhydrophobic SERS platform can potentially allow an analyte solution of equal concentration and volume to be concentrated at least 58.9-fold than on a hydrophilic substrate, therefore improving SERS sensitivity for ultratrace molecular sensing.

We evaluate the performance of our superhydrophobic SERS platform for ultratrace molecular sensing by determining the SERS responses of rhodamine 6G on the surface. All SERS spectra obtained from 4 μL of various concentrations of rhodamine 6G, ranging from 10^{-17} M to 10^{-7} M, exhibit characteristic vibrational features at 610, 772, 1182, 1308, 1358 and 1504 cm^{-1} (Figure 5a, Figure S4).³¹⁻³³ The most intense SERS band at 610 cm^{-1} is selected for comparison across various concentrations of rhodamine 6G. Initially, at high rhodamine 6G concentration of 10^{-7} M, a SERS intensity of 9894 ± 1216 counts is obtained. A 10^4 -fold dilution of rhodamine 6G to 10^{-11} M decreases the SERS intensity to 703 ± 151 counts. As the analyte solutions are further diluted, the SERS intensities decreases and eventually reaching 175 ± 30 counts at a rhodamine 6G concentration of 10^{-17} M (Figure 5b, Figure S5). We would like to emphasize that all SERS spectra obtained show distinguishable signals at 610 cm^{-1} , with a signal-to-noise ratio > 3 even at 10^{-17} M of rhodamine 6G. Any further dilution resulted in a signal-to-noise ratio < 3 and is considered indistinguishable from the background noises. The detection limit of our superhydrophobic SERS platform is therefore determined to be 10^{-17} M of rhodamine 6G. A control analysis of the superhydrophobic SERS platform in the absence of rhodamine 6G yields a featureless SERS spectrum in the Raman window of interest (“control” of Figure 5b). This further affirms that the SERS signal at 610 cm^{-1} , even at 10^{-17} M of rhodamine 6G, is due solely to the analyte molecules and also perfluorodecanethiol molecules do not interfere significantly with the ultratrace sensing application of our superhydrophobic SERS platform.

Quantitative comparison of the SERS intensities across various rhodamine 6G concentrations demonstrates that when the concentration of rhodamine 6G is within the range 10^{-7} to 10^{-11} M (Figure 5c), a linear SERS response is obtained. This observation is agreeable to previously reported

studies involving homogenous SERS substrate hence highlights the suitability of our superhydrophobic SERS platform for quantitative detection of analyte molecules. Below 10^{-11} M of rhodamine 6G, we observe that the SERS intensities remain relatively constant, even after a 10^6 -folds dilution to 10^{-17} M of rhodamine 6G. The similar SERS responses with decreasing analyte concentrations can be attributed to the Langmuir adsorption isotherm of physically-adsorbed rhodamine 6G. Rhodamine 6G concentrations $< 10^{-11}$ M can be approximated to the submonolayer adsorption of analyte aggregates such that SERS signals are obtained from individual submonolayer aggregates, leading to constant SERS intensities despite changes in analyte concentrations. Nevertheless, the ability to detect submonolayer analyte aggregates, even at attomolar level, is a strong demonstration of the superiority of our superhydrophobic SERS platform, with an analyte concentrating factor of 57-folds, over conventional hydrophilic platforms.

High SERS signal homogeneity and repeatability of our superhydrophobic SERS platform are further demonstrated via its SERS imaging. Using the SERS image at 10^{-9} M rhodamine 6G as an example and by selecting its characteristic SERS band at 610 cm^{-1} , our superhydrophobic SERS platform clearly shows uniform SERS signal (Figure 6a) across the region where rhodamine 6G is deposited after drying. Evaluation of 20 SERS spectra randomly collected across the scanned area (Figure 6b) reveals an average SERS intensity of 1892 ± 151 counts (Figure 6c), corresponding to a relative standard deviation of 8%. Such low relative standard deviation of $< 10\%$ is in close agreement to other homogeneous SERS platforms,^{34, 35} thus highlighting the high repeatability of SERS response on our superhydrophobic platform for quantitative and ultratrace molecular detection.

Analytical enhancement factor (AEF) is calculated to quantify the improvement of SERS enhancement of analyte molecules concentrated on our superhydrophobic SERS substrate as compared to hydrophilic normal Raman platform. Analytical EF is defined as: $AEF = [(I_{\text{SERS}}) / (I_{\text{Raman}})] \times [(C_{\text{Raman}}) / (C_{\text{SERS}})]$, where I_{SERS} and I_{Raman} are signals collected from SERS and normal Raman platform respectively; C_{SERS} and C_{Raman} are the corresponding lowest concentration measurable on the superhydrophobic SERS platform and hydrophilic normal Raman platform respectively. Based on the signal at 610 cm^{-1} , an analytical enhancement factor of 2×10^{13} is

achieved using our superhydrophobic SERS platform (Figure S4), which is at least 100-folds more sensitive than other superhydrophobic SERS platform reported.^{13,21} By providing at least 10^{13} -fold enhancement of signal intensity, as compared to a hydrophilic normal Raman platform, our superhydrophobic SERS platform is clearly demonstrated to possess superior detection sensitivity essential for ultratrace molecular sensing, especially in the field of criminology and industrial and environmental safety.

Summing up, we have demonstrated a cost- and time-effective approach to fabricate homogeneous large scale superhydrophobic platform with SERS detection capability down to attomolar level (10^{-17} M) of rhodamine 6G. With the aid of superhydrophobicity to enhance localization of analyte molecules, analyte volumes of just 4 μ L are required which make our superhydrophobic SERS platform highly attractive as an analytical platform in miniaturized devices, such as lab-on-a-chip system. Furthermore, our protocols are also generic and can be extended to other polymers, periodic patterns and materials/morphologies of plasmonic nanocrystal to tailor both the physical and plasmonic properties of the superhydrophobic SERS platforms. With the ensemble of benefits, the large-scale fabrication of homogeneous superhydrophobic SERS platforms will open up opportunities in ultratrace detection of toxins and/or molecules in the field of safety, criminology, and even routine industrial applications.

Experimental Details

Chemicals. Silver nitrate ($\geq 99\%$), anhydrous 1,5-pentanediol ($\geq 97\%$), poly(vinylpyrrolidone) (average MW = 55,000), poly (methyl methacrylate) (PMMA, average MW 350,000), 1H,1H,2H,2H-perfluorooctyltriethoxysilane ($\geq 98\%$), 1H,1H,2H,2H-perfluorodecanethiol (PFDT, $\geq 97\%$), rhodamine 6G (R6G, dye content $\sim 95\%$) were purchased from Sigma-Aldrich; copper (II) chloride ($\geq 98\%$) was from Alfa Aesar; ethanol (ACS, ISO, Reag. Ph Eur) was from EMSURE®; hexane (AR grade) was purchased from JT Baker; toluene (AR grade) was from Fisher Chemicals. Milli-Q water (≥ 18.0 M Ω . cm) was purified with a Sartorius Arium® 611 UV ultrapure water

system. Tri-methyl aluminium (TMA, electronic grade) is purchased from SAFC Taiwan. All chemicals were applied without further purification.

Spin coating. Silicon wafers (1.5 cm × 1.5 cm) were first washed with piranha solution and O₂-plasma cleaned before use. 10 wt % PMMA/toluene is prepared and diluted to 4 wt % PMMA/toluene before use. 200 μL of the as-prepared solution is evenly dripped on the cleaned Si substrate and spinned at 2000 rpm with an acceleration of 5000 m/s² for 30s using a Spin 150 machine. The wafers were then baked on a hot plate at 80 °C for 10 minutes to evaporate the residual solvent and 200 nm PMMA films were obtained.

Nanoimprint lithography. A linear stamp features (1.5 cm × 1.5 cm wafer with a 1 × 1 cm pattern (linear arrays of 1 μm height, 3 μm width and 7 μm periodicity) in the center, was treated with 1H,1H,2H,2H-perfluorooctyltriethoxysilane to lower the surface energy and prevent adhesion. The treated stamp was then used to imprint the linear patterns on the polymer layer by applying pressure of 2 × 10³ N at a temperature of 200°C, which is above the glass transition temperature of PMMA, with a Specac heat press. The substrate was heated in the heat press for a period of five minutes to increase fluidity of PMMA before pressure was applied for 20 minutes. This imprinting process was repeated on the same substrate, rotated at 90°, to achieve a cross imprint. To protect the polymeric pillars, a layer of inert aluminium oxide (Al₂O₃, 10 nm) was coated via atomic layer deposition (ALD, Picosun SUNALE™ R-150). The substrate was then O₂-plasma treated (5 min, 50 W).

Synthesis and purification of Ag nanocubes. The preparation of Ag nanocubes was carried out following the method described in literature. Briefly, 10 mL of copper (II) chloride (8 mg/mL), poly(vinylpyrrolidone) (20 mg/mL) and silver nitrate (20 mg/mL) were separately dissolved in 1,5-pentanediol. The chemicals were sonicated and vortexed repeatedly to dissolve them. 35-μL copper (II) chloride solution was then added to the silver nitrate solution. Then, 20-mL 1,5-pentanediol in a 100-mL round bottomed flask was heated to 190° C for 10 min. 250-μL poly(vinylpyrrolidone) precursor was added to flask dropwise every 30 s while 500-μL silver nitrate precursor was injected

every min using a quick addition. The addition process continued until the greenish coloration of the reaction mixture faded off.

For the purification of Ag nanocubes, 1,5-pentanediol was first removed from the mixture through centrifugation. The Ag nanocubes solution was then dispersed in 10-mL ethanol and 100-mL aqueous poly(vinylpyrrolidone) solution (0.2 g/L). The resulting solution was vacuum filtered using polyvinylidene fluoride filter membranes (Sigma Alrich) with pore sizes ranging from 5000 nm, 650 nm, 450 nm and 220 nm, repeated several times for each pore size. SEM imaging was performed, from which the edge lengths of 100 Ag nanocubes were measured and analyzed using ImageJ software.

Assembly of Silver nanocubes using Langmuir-Schaefer technique. Purified Ag nanocubes were dispersed in 2:3 ethanol/chloroform solution and dispersed on the surface of water. The monolayer of Ag nanocubes was then transferred onto Si substrate via the Langmuir-Schaefer method and blow-dried with N₂ gas.

Preparation of superhydrophobic surface. Cr and Ag films were deposited using a home-built thermal evaporator deposition system. 2-nm Cr adhesion layer was first deposited, followed by 25-nm Ag film. The deposition rates of the films were 0.1 Å/s and 0.5 Å/s, respectively, which was monitored in-situ by a quartz crystal microbalance. The substrate was then functionalized via immersion into a 1:1 ethanol/hexane solution of 1H,1H,2H,2H-perfluorodecanethiol (5 mM, 15 h).

Analysis of rhodamine 6G on as-prepared SERS substrate. Rhodamine 6G (4.79 mg/mL, 10⁻² M) was prepared in aqueous solution using ultrapure water and subsequently diluted to give a series of concentrations, ranging from 10⁻⁷ M to 10⁻¹⁷ M. 4-μL droplets of each rhodamine 6G concentrations were placed on the superhydrophobic SERS substrate. The droplets were allowed to dry under ambient condition and then subjected to SERS characterization.

Characterization. SEM imaging was performed using a JEOL-JSM-7600F microscope. Contact angles were measured with an Attension tensiometer equipped with a Firewire digital camera. Static contact angles were measured with 4-μL of ultrapure water. Advancing and receding contact angles

were determined using drop shape analysis routine of a growing and shrinking drop of water respectively. The root-mean-square roughness of the as-prepared substrates was measured using JPK Nanowizard®3 BioScience atomic force microscopy (AFM) on a Zeiss inverted microscope. Silicon cantilevers from Budgetsensors (model Tap300-G with 30-nm Aluminum back reflex coating) were used for non-contact mode operation. All contact angles were averaged over 5 measurements performed at different spots for each substrate. SERS measurements were performed using x-y imaging mode of the Ramantouch microspectrometer (Nanophoton Inc, Osaka, Japan) with an excitation wavelength of 532 nm (power = 23 μ W). A 20 \times (N.A. 0.45) objective lens with 1 s accumulation time was used for data collection between 200 cm^{-1} to 1800 cm^{-1} . All SERS spectra collected are baseline-corrected using a 5th order polynomial equation via the Raman viewer software provided by Nanophoton Inc. All SERS spectra were obtained by averaging at least 25 individual spectra.

Acknowledgements

X.Y.L. thanks the support from National Research Foundation, Singapore (NRF-NRFF2012-04), and Nanyang Technological University's start-up grant (M4080758). J.M.R.T. thanks the graduate scholarship from Interdisciplinary Graduate School, NTU, Singapore. H.K.L. thanks the A*STAR Graduate Scholarship support from A*STAR, Singapore.

References

1. P. Etchegoin, R. C. Maher, L. Cohen, H. Hartigan, R. Brown, M. Milton and J. Gallop, *Chem. Phys. Lett.*, 2003, 375, 84-90.
2. B. Wang, L. Zhang and X. Zhou, *Spectrochimica Acta Part A: Molecular and Biomolecular Spectroscopy*, 2014, 121, 63-69.
3. J. A. Dieringer, A. D. McFarland, N. C. Shah, D. A. Stuart, A. V. Whitney, C. R. Yonzon, M. A. Young, X. Zhang and R. P. Van Duyne, *Faraday Discuss.*, 2006, 132, 9-26.
4. S. Gao, H. Zhang, X. Wang, J. Yang, L. Zhou, C. Peng, D. Sun and M. Li, *Nanotechnology*, 2005, 16, 2530.
5. W. Xie, P. Qiu and C. Mao, *J. Mater. Chem.*, 2011, 21, 5190-5202.
6. A. Campion and P. Kambhampati, *Chem. Soc. Rev.*, 1998, 27, 241-250.
7. G. C. Schatz, M. A. Young and R. P. Van Duyne, in *Surface-enhanced Raman scattering*, Springer, 2006, pp. 19-45.

8. L. Qin, S. Zou, C. Xue, A. Atkinson, G. C. Schatz and C. A. Mirkin, *Proc. Natl. Acad. Sci.*, 2006, 103, 13300-13303.
9. G. Braun, I. Pavel, A. R. Morrill, D. S. Seferos, G. C. Bazan, N. O. Reich and M. Moskovits, *J. Am. Chem. Soc.*, 2007, 129, 7760-7761.
10. J. P. Camden, J. A. Dieringer, Y. Wang, D. J. Masiello, L. D. Marks, G. C. Schatz and R. P. Van Duyne, *J. Am. Chem. Soc.*, 2008, 130, 12616-12617.
11. R. Aroca, C. Jennings, G. J. Kovac, R. O. Loutfy and P. S. Vincett, *J. Phys. Chem.*, 1985, 89, 4051-4054.
12. N. Pazos-Perez, C. S. Wagner, J. M. Romo-Herrera, L. M. Liz-Marzán, F. J. García de Abajo, A. Wittemann, A. Fery and R. A. Alvarez-Puebla, *Angew. Chem., Int. Ed.*, 2012, 51, 12688-12693.
13. B. B. Xu, Y. L. Zhang, W. Y. Zhang, X. Q. Liu, J. N. Wang, X. L. Zhang, D. D. Zhang, H. B. Jiang, R. Zhang and H. B. Sun, *Advanced Optical Materials*, 2013, 1, 56-60.
14. F. Xu, Y. Zhang, Y. Sun, Y. Shi, Z. Wen and Z. Li, *J. Phys. Chem. C*, 2011, 115, 9977-9983.
15. H. K. Lee, Y. H. Lee, Q. Zhang, I. Y. Phang, J. M. R. Tan, Y. Cui and X. Y. Ling, *ACS Appl. Mater. Interfaces*, 2013, 5, 11409-11418.
16. X.-M. Li, D. Reinhoudt and M. Crego-Calama, *Chem. Soc. Rev.*, 2007, 36, 1350-1368.
17. L. Zhai, M. C. Berg, F. C. Cebeci, Y. Kim, J. M. Milwid, M. F. Rubner and R. E. Cohen, *Nano Lett.*, 2006, 6, 1213-1217.
18. L. Feng, S. Li, Y. Li, H. Li, L. Zhang, J. Zhai, Y. Song, B. Liu, L. Jiang and D. Zhu, *Adv. Mater.*, 2002, 14, 1857-1860.
19. Z. Chen, L. Hao, A. Chen, Q. Song and C. Chen, *Electrochim. Acta*, 2012, 59, 168-171.
20. F. Gentile, M. L. Coluccio, N. Coppedè, F. Mecarini, G. Das, C. Liberale, L. Tirinato, M. Leoncini, G. Perozziello and P. Candeloro, *ACS Appl. Mater. Interfaces*, 2012, 4, 3213-3224.
21. F. De Angelis, F. Gentile, F. Mecarini, G. Das, M. Moretti, P. Candeloro, M. Coluccio, G. Cojoc, A. Accardo and C. Liberale, *Nat. Photonics*, 2011, 5, 682-687.
22. C. M. Bruinink, M. Péter, P. A. Maury, M. De Boer, L. Kuipers, J. Huskens and D. N. Reinhoudt, *Adv. Funct. Mater.*, 2006, 16, 1555-1565.
23. M. J. Mulvihill, X. Y. Ling, J. Henzie and P. Yang, *J. Am. Chem. Soc.*, 2009, 132, 268-274.
24. L. J. Sherry, S.-H. Chang, G. C. Schatz, R. P. Van Duyne, B. J. Wiley and Y. Xia, *Nano Lett.*, 2005, 5, 2034-2038.
25. B. Valter, M. K. Ram and C. Nicolini, *Langmuir*, 2002, 18, 1535-1541.
26. M. K. Ram, M. Adami, M. Sartore, M. Salerno, S. Paddeu and C. Nicolini, *Synth. Met.*, 1999, 100, 249-259.
27. N. J. Shirtcliffe, G. McHale, S. Atherton and M. I. Newton, *Adv. Colloid Interface Sci.*, 2010, 161, 124-138.
28. H. Y. Erbil and C. E. Cansoy, *Langmuir*, 2009, 25, 14135-14145.
29. R. N. Wenzel, *Industrial & Engineering Chemistry*, 1936, 28, 988-994.
30. A. B. D. Cassie and S. Baxter, *Trans. Faraday Soc.*, 1944, 40, 546-551.
31. L.-Q. Lu, Y. Zheng, W.-G. Qu, H.-Q. Yu and A.-W. Xu, *J. Mater. Chem.*, 2012, 22, 20986-20990.
32. P. Hildebrandt and M. Stockburger, *J. Phys. Chem.*, 1984, 88, 5935-5944.
33. Z. Huang, G. Meng, Q. Huang, Y. Yang, C. Zhu and C. Tang, *Adv. Mater.*, 2010, 22, 4136-4139.
34. H. Liu, X. Zhang, T. Zhai, T. Sander, L. Chen and P. J. Klar, *Nanoscale*, 2014, 6, 5099-5105.
35. Q. Zhang, Y. H. Lee, I. Y. Phang, C. K. Lee and X. Y. Ling, *Small*, 2014, 10, 2703-2711.

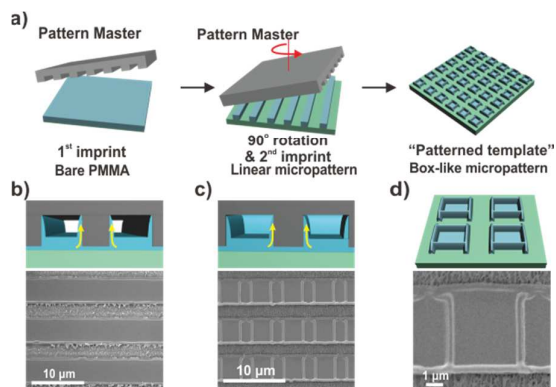


Figure 1. Fabrication of large-scale box-like patterned polymeric periodic arrays using capillary force lithography. (a) Scheme of the capillary force lithography fabrication process to obtain polymeric periodic arrays. SEM images of (b) linear pattern upon first nanoimprinting process and (c and d) box-like patterned template after second nanoimprinting by 90° rotation of the Si master.

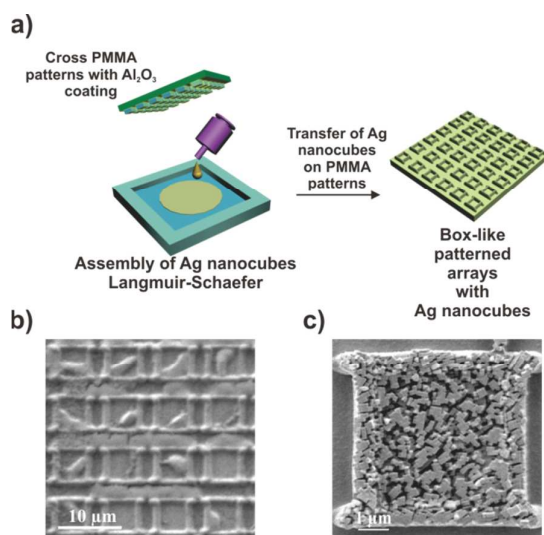


Figure 2. (a) Decoration of Ag nanocubes onto as-prepared patterned template. (b) Low magnification and (c) high magnification SEM image of box-like pattern arrays with Ag nanocubes.

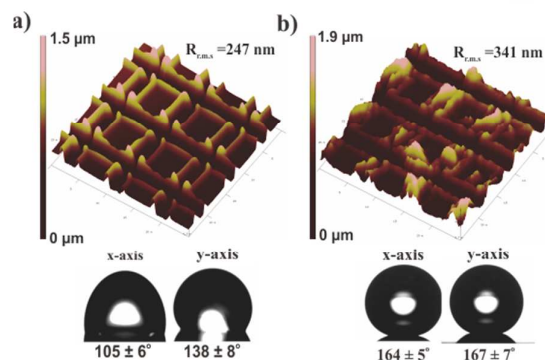


Figure 3. AFM images of root mean square of surface roughness (r.m.s.) and contact angle for (a) bare polymeric patterned array and (b) Ag nanocube-decorated patterned template.

Table 1. Tabulation of average surface roughness, static and dynamic contact angles and contact angle hysteresis at various stages of nanoimprinting process.

	Sample	Surface roughness (nm)		Contact angle (°)			
				Static	Advancing	Receding	Hysteresis
	Flat PMMA (with PFDT)	0.296		111 ± 4	119 ± 4	88 ± 8	31 ± 9
	Linear micropatterns (with PFDT)	167	X-axis	124 ± 5	128 ± 3	85 ± 11	43 ± 11
			Y-axis	157 ± 5	162 ± 5	117 ± 3	45 ± 6
	Box-like micropatterns (with PFDT)	247	X-axis	106 ± 5	105 ± 6	66 ± 9	40 ± 7
			Y-axis	138 ± 9	136 ± 8	91 ± 10	47 ± 5
	Box-like micropatterns with AgNCs (with PFDT)	341	X-axis	165 ± 9	164 ± 5	130 ± 3	35 ± 9
			Y-axis	168 ± 2	167 ± 7	130 ± 3	38 ± 4
	Box-like micropatterns with AgNCs (without PFDT)	341	X-axis	143 ± 2	144 ± 8	87 ± 8	57 ± 11
			Y-axis	139 ± 2	140 ± 5	89 ± 4	51 ± 6

*AgNCs – Silver nanocubes

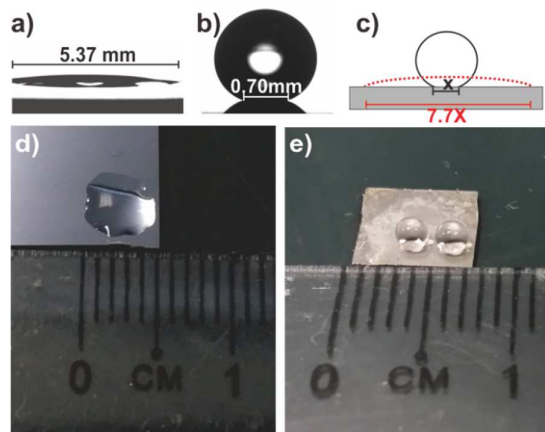


Figure 4. Concentrating effect on the superhydrophobic surface. Static contact angle images of 4 μL water droplets on (a) hydrophilic O_2 -plasma treated surface and (b) superhydrophobic SERS platform. (c) Schematic comparing maximum contact area on the superhydrophobic surface and hydrophilic surface. Optical images of the sessile water droplets on (d) hydrophilic surface and e) superhydrophobic surface.

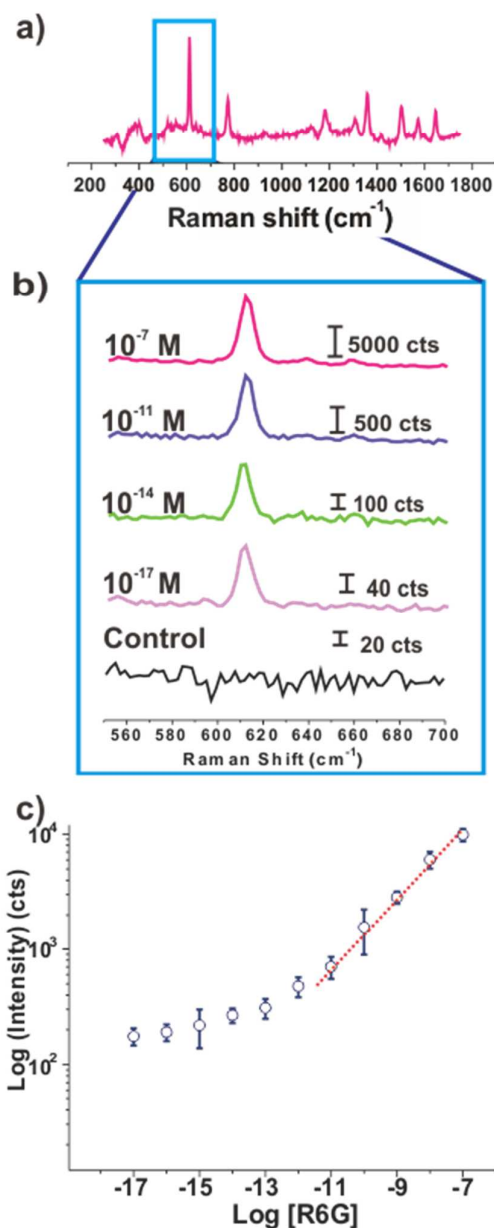


Figure 5. Application of superhydrophobic SERS platform for ultratrace analysis using rhodamine 6G as probe molecule. (a) SERS spectrum of rhodamine 6G on superhydrophobic SERS platform. (b) Magnified SERS spectra of rhodamine 6G with concentrations ranging from 10^{-17} to 10^{-7} M. (c) SERS intensities at 610 cm^{-1} for rhodamine 6G concentrations ranging from 10^{-17} to 10^{-7} M. Error bars are obtained with 25 repeated trials.

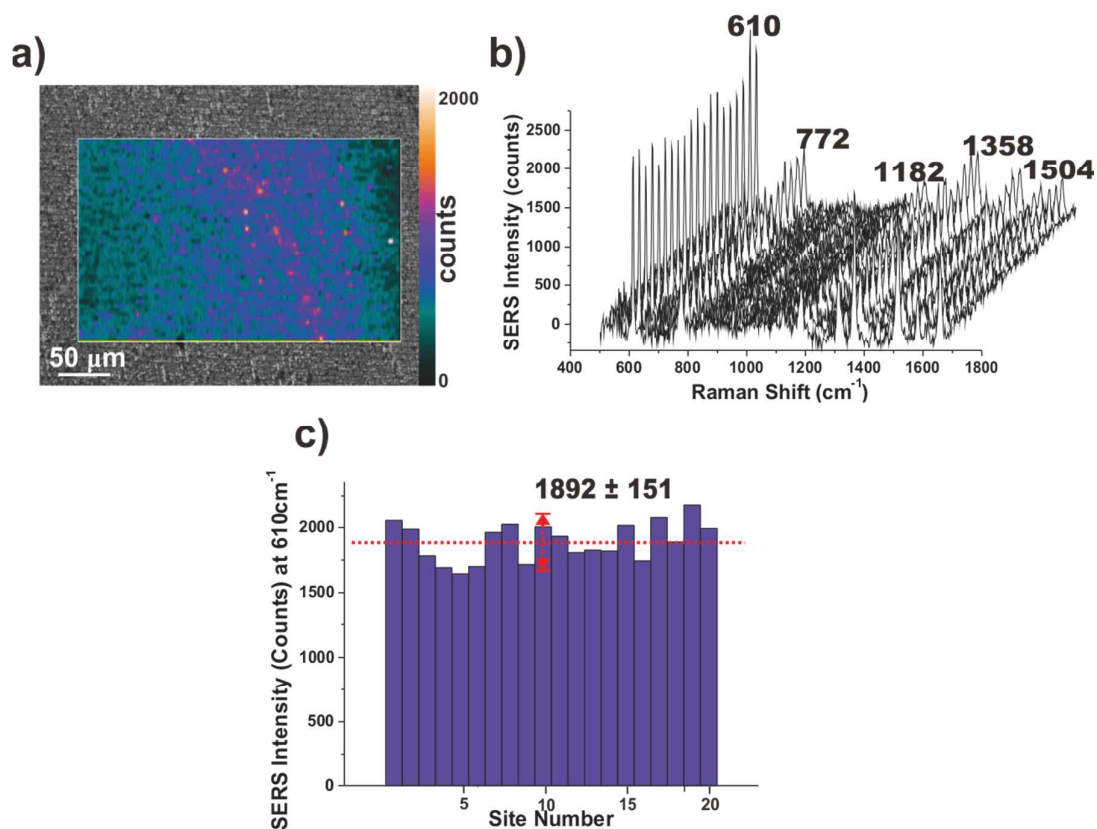


Figure 6. Evaluation of SERS signal repeatability on superhydrophobic SERS platform using dried rhodamine 6G (4 μL , 1 nM). a) SERS image overlaid with its optical image, b) 20 SERS spectra collected randomly across the scanned area. c) Comparison of SERS intensity on superhydrophobic SERS platform using the 20 SERS spectra from (b). The SERS image is obtained by selecting the SERS band at 610 cm^{-1} .